

Operando Raman Spectroscopy: Studies on the Reactivity and Stability of SnO₂ Nanoparticles During Electrochemical CO₂ Reduction Reaction

A Kuzume, Tokyo Institute of Technology, Yokohama, Japan

A Dutta, University of Bern, Bern, Switzerland

S Veszteg, Eötvös Loránd University, Budapest, Hungary

P Broekmann, University of Bern, Bern, Switzerland

© 2018 Elsevier Inc. All rights reserved.

Electrochemical Reduction of CO ₂	217
Electrochemical Reduction of CO ₂ on Tin Electrode	218
Faradaic Efficiency of CO ₂ Electroreduction for Formate Formation	219
Sn/SnO ₂ Nano-Catalysts for CO ₂ Electroreduction	219
Monitoring the Electrochemical Reduction of CO ₂ on Sn/SnO ₂	220
Operando Raman Study on Electrochemical Reduction of CO ₂	220
Conclusion	223
References	223
Further Reading	225

Nomenclature

CO ₂	Carbon dioxide
FE	Faradaic efficiency
Sn	Tin
SnO ₂	Tin(IV) oxide
SnO	Tin(II) oxide

Electrochemical Reduction of CO₂

Today there is a consensus within the scientific community that the huge increase of carbon dioxide (CO₂) concentration in the atmosphere is due to anthropogenic sources such as the burning of fossil fuels and the destruction of forests. The current production of CO₂ by human activity seems to exceed the capacity of the planet to consume CO₂ by photosynthesis and oceanic absorption. Thus the balance of the global CO₂ cycle of the atmosphere is in a crucial condition.

The growing CO₂ content in the atmosphere and additional anthropogenic activity has captured noticeable attention in the past century, mostly due to the significant effects on the global climate.^{1–3} Consequently, a number of technologies including capture and sequestration of CO₂ have been developed to decrease the level of CO₂ content in the air.^{4–9} Among these, the number of literature reports dealing with the electrochemical reduction of CO₂ in particular^{10–22} is constantly rising, ever since it was first described by the pioneering work of Royer in 1870.²³

In principle, the electrochemical reduction of CO₂ can be performed in common electrolyzing cells.⁹ The anode reaction in a CO₂ electrolysis device is very often the oxidation of water (yielding oxygen molecules), whereas the cathode reaction is the reduction of CO₂ (usually dissolved in an aqueous electrolyte). The electrochemical reduction of CO₂ involves multiple proton-coupled electron transfer steps, yielding various products such as CO, formate, hydrocarbons (CH₄, C₂H₄, C₂H₆), and alcohols (CH₃OH, C₂H₅OH, 1-propanol) in aqueous media. Naturally, in aqueous media hydrogen evolution must always be considered as a side reaction competing with CO₂ electroreduction.

Converting CO₂ selectively to a specific reaction product is a challenging task that can be achieved by the choice of proper catalysts. In the 1980s, Hori et al. published a comparative study on electrochemical CO₂ reduction at different metal electrodes. They reported different overall activities and product distributions which they attempted to explain based on the different chemical nature of the cathode materials.²⁴ Hori et al. roughly categorized metals into two groups, based on their CO₂ conversion products (Table 1). They distinguished metals where the main product of CO₂ electroreduction is CO (Cu, Au, Ag, Pt, Pd, Zn, Ni, and Ga) from metals where the main product is formate (Hg, Pb, Tl, Cd, In, Sn). The generation of CO₂^{•–} in the first step is often rate limiting in the CO₂ electroreduction process and it is the coordination of this intermediate which determines whether the 2e[–] reduction product will either be CO or formate.²⁵

Hori et al. proposed mechanisms for CO₂ electroreduction for both above-mentioned groups of metals. In case of the former group (where the main product is CO), the reaction intermediate CO₂^{•–} is formed by an initial electron transfer from the electrode

Table 1 Various products from the electroreduction of CO₂ in 0.1 M KHCO₃. Reprint with permission from ref. 24. Copyright 1994, with permission from Elsevier.)

Electrode	Potential vs. NHE/V	Curr. dens./ (mA cm ⁻²)	Faradaic efficiency/%							
			CH ₄	C ₂ H ₄	EtOH	PrOH	CO	HCOO ⁻	H ₂	Total
Cu	-1.44	5.0	33.3	25.5	5.7	3.0	1.3	9.4	20.5	103.5 ^a
Au	-1.14	5.0	0.0	0.0	0.0	0.0	87.1	0.7	10.2	98.0
Ag	-1.37	5.0	0.0	0.0	0.0	0.0	81.5	0.8	12.4	94.6
Zn	-1.54	5.0	0.0	0.0	0.0	0.0	79.4	6.1	9.9	95.4
Pd	-1.20	5.0	2.9	0.0	0.0	0.0	28.3	2.8	26.2	60.2
Ga	-1.24	5.0	0.0	0.0	0.0	0.0	23.2	0.0	79.0	102.0
Pb	-1.63	5.0	0.0	0.0	0.0	0.0	0.0	97.4	5.0	102.4
Hg	-1.51	0.5	0.0	0.0	0.0	0.0	0.0	99.5	0.0	99.5
In	-1.55	5.0	0.0	0.0	0.0	0.0	2.1	94.9	3.3	100.3
Sn	-1.48	5.0	0.0	0.0	0.0	0.0	7.1	88.4	4.6	100.1
Cd	-1.63	5.0	1.3	0.0	0.0	0.0	13.9	78.4	9.4	103.0
Tl	-1.60	5.0	0.0	0.0	0.0	0.0	0.0	95.1	6.2	101.3
Ni	-1.48	5.0	1.8	0.1	0.0	0.0	0.0	1.4	88.9	92.4 ^b
Fe	-0.91	5.0	0.0	0.0	0.0	0.0	0.0	0.0	94.8	94.8
Pt	-1.07	5.0	0.0	0.0	0.0	0.0	0.0	0.1	95.7	95.8
Ti	-1.60	5.0	0.0	0.0	0.0	0.0	Traces	0.0	99.7	99.7

^aThe total value contains C₃H₅OH (1.4%), CH₃CHO (1.1%), and C₂H₅CHO in addition to the tabulated substances.^bThe total value contains C₂H₆ (0.2%).

metal to the CO₂ molecules adsorbed at the surface.²⁶ This is chemically equivalent to CO₂ coordinating with transition metal atoms.²⁷ In this case, the adsorbed intermediate is stabilized by a back donation of electrons from the d orbitals of the metal atoms to the antibonding π^* orbital of CO₂. The extra negative charge on the O atom will then promote protonation to form CO and water.

In case of the latter metal group (where the favored reaction product is formate), the reaction intermediate is present in the electrolyte solution,²⁸ where the density of unpaired electrons is high on the C atom.²⁹ Thus the intermediate will react with protons from the electrolyte to form formate.

As opposed to most metals where CO₂ electroreduction remains a 2e⁻ process (yielding formate or CO), Cu electrodes also favor multiple electron processes. On Cu, CO₂ can be converted to many types of C1 and C2 hydrocarbons (such as CH₄ and C₂H₄) as well as to alcohols.^{24,30}

Apart from pure metals, metal alloys, and oxides may also be used as efficient catalysts for the electroreduction of CO₂.^{4,31–48} Earlier, Azuma et al. reported product distributions on different metal catalysts in aqueous solution.⁴⁹ Recently, Qiao et al. classified metal alloys, metal complexes, and metal oxides based on their activity (and selectivity) toward electrochemical CO₂ reduction.⁵⁰ Kanan et al. published a number of reports on CO₂ electroreduction on metal oxide, especially tin oxide systems.^{51–53} White et al. recently reported high electrocatalytic activity toward CO₂ electroreduction measured on In/In₂O₃ nanoparticles with a faradaic efficiency (FE) of 50%–80% toward the production of formate.⁵⁴

Electrochemical Reduction of CO₂ on Tin Electrode

Among other metals favoring the production of formate (Table 1) indium^{54–56} and tin^{57–62} deserve attention due to their high activity and low cost compared to platinum group and coinage metals. In addition, In and Sn are less toxic compared to some other formate-producing metals (Hg, Pb, Tl, and Cd).

Although Sn itself is generally described as an electrode material at which the production of formate is favored: the product selectivity and the overall reaction efficiency may however depend on many experimental conditions. In particular, the selectivity for the production of formate highly depends on the pretreatment of Sn electrodes. Kanan et al. found an exclusive formation of hydrogen gas on freshly etched Sn surfaces, showing that the presence of oxide (in a general form: SnO_x) is essential for efficient CO₂ reduction and the production of formate.⁵² Wu et al. prepared SnO_x electrodes by reducing an SnO_x layer after 20 min of preelectrolysis affecting the product selectivity.⁶³

Lei et al. pointed out that etching Sn surfaces by HCl(aq) roughens the electrode surface, and the surface oxide layer can however be restored by exposure to air for 24 h. This reduction–reoxidation pretreatment leads to a 1.5-fold increment of the achievable current density, compared to untreated bare Sn electrodes.⁵⁷

Cui et al. performed density functional theory calculations to understand the role of SnO_x in CO₂ reduction. Their model system considered an SnO monolayer on an Sn(112) model surface.⁴⁷ They described a scenario according to which hydroxyl groups (formed by a dissociative adsorption of water molecules on the SnO monolayer) react with CO₂ to form a bicarbonate intermediate, which can be further reduced to formate.

Apart from the oxidation state of Sn surfaces, the composition of the electrolyte may also play a decisive role as to the selectivity and activity of electrochemical CO₂ reduction on Sn surfaces.⁶⁴

Faradaic Efficiency of CO₂ Electroreduction for Formate Formation

The electroreduction of CO₂ on tin and tin-related electrode materials shows wide discrepancies in terms of the reported FEs of formate production. According to literature, FE values range between 5% and 90%.^{11,14,65–69} The variation in the FE values implies that the electro-catalytic activity of Sn depends on many experimental conditions, such as its morphology,^{70,71} chemical and oxidation state,^{72–74} temperature,^{75,76} CO₂ pressure/concentration,⁷⁷ overpotentials,⁷⁸ and the pH of the electrolyte solution.⁷⁹ This is also supported by some recent studies focusing on the variation of product distribution as a function of pH^{14,58,80,81} or as a result of surface deactivation.

It is reported that the FE for formate production on Sn/Zn electrode in a fixed-bed reactor containing CO₂-saturated aqueous KHCO₃ solution is 90% for 30 min, but it dropped down to 30% after 2 h. This peculiar FE drop was first explained by the oxidation of formic acid on the anode.⁶⁰ However, another report explained that FE drops might also be caused by the deposition of Zn on the Sn surface together with the degradation of electrode materials during electrolysis.⁶⁵

Sridhar et al. investigated the cathodic degradation mechanism of pure Sn electrodes during CO₂ electrolysis by using rotating disk electrodes, investigating the effect of electrolyte concentration, time, current density, and surface orientation.⁵⁸ Further studies by the same group on the degradation and deactivation mechanism of Sn catalysts for CO₂ electroreduction reveal that the optimum potential for CO₂ reduction on Sn electrodes is -1.8 V (vs. SCE), where the FE reaches its maximum while the degradation is minimal.⁷⁸ Here, two types of degradation processes were proposed: cathodic corrosion and deposition of alkali metal (KSn). The former type of degradation did not cause deactivation in FE, while the latter, which occurred during simultaneous CO₂ reduction, led to severe cathodic deactivation and material losses.

Bumroongsakulsawat and Kelsall studied the dependence of the molar ratios of CO and formate formed by electroreduction of CO₂ on Sn electrode as a function of solution pH.⁸⁰ A mathematical model was developed to predict the relationship between the product ratio and pH, revealing the individual partial current densities for both formate and CO formation in the ranges of potential and pH studied. These authors concluded that the solution pH appeared to affect the distribution of three adsorbed intermediates, CO₂^{•-}, COOH, and COOH⁺, by protonation, which control the product ratio.

More recently, Lee et al. performed CO₂ reduction on SnO₂ in alkaline media to investigate the effect of pH and applied potential on the catalytic performance of SnO₂ electrodes in terms of activity, selectivity, and stability of the oxide phase.⁸² They showed that the pH of the solution determines the equilibrium concentration of the bicarbonate/carbonate system, as well as the thermodynamically stable phase of tin dioxide. They concluded that optimizing the solution pH offers distinct advantage in achieving better activity, selectivity, and stability (Fig. 1).

Sn/SnO₂ Nano-Catalysts for CO₂ Electroreduction

A few studies dealing with CO₂ reduction on nanoparticulate tin oxide have surfaced in the past years.^{63,83–86} Del Castillo et al. studied the effect of Sn particle size and metal loading on the electrolysis current density using electrochemical methods.⁷⁰ They found that Sn particles with an average size of 150 nm displayed the best performance, achieving high rates of formate production with FEs of around 70%. This is close to the performance required to operate an industrial electrochemical process. On the other hand, Zhang et al. reported that high-surface-area graphene-supported tin oxide nanocrystals having 5 nm particle sizes have 93% conversion efficiency toward formate production.⁸³

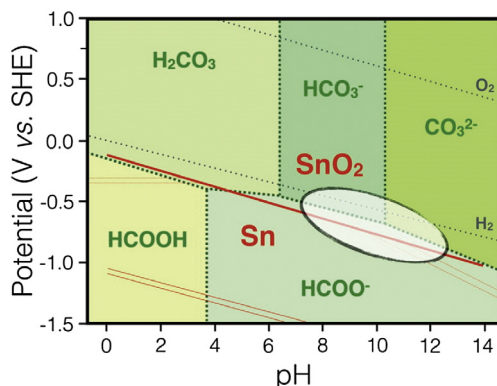


Fig. 1 Combined potential-pH equilibrium diagram of the Sn-water system considering oxide phase and carbonate-water system. The encircled area indicates the overlap region where stable SnO₂ phase could catalyse formate formation from CO₂. Reprinted with permission from Lee, S.; Ocon, J.D.; Son, Y.; Lee, J. Alkaline CO₂ Electrolysis Toward Selective and Continuous HCOO⁻ Production Over SnO₂ Nanocatalysts. *J. Phys. Chem. C* **2015**, *119*, 4884–4890. Copyright 2015, American Chemical Society.

Monitoring the Electrochemical Reduction of CO₂ on Sn/SnO₂

Recently, Bocarsly et al. applied in situ ATR-IR spectroscopy for studying the mechanism of CO₂ reduction on tin films covered by SnO_x.^{87,88} Thin films of mixed Sn/SnO_x content were deposited on the ATR crystal, where monodentate tin carbonate species were consistently present in the course of CO₂ reduction (Fig. 2). These peaks disappeared in low pH solutions or on metallic tin surface. They concluded that the oxidation state of the tin catalyst cannot always be maintained at the highly cathodic operating conditions,^{61,89} and the reduction of SnO₂ often results in a decreased FE for formate production.

It is still a challenging task to monitor simultaneous dynamic changes in the structural and chemical properties of heterogeneous nanostructured catalyst surface during electrolysis in real-life reactors. A detailed characterization of catalyst properties under reaction condition is necessary for designing nano-catalysts with high activity, selectivity, and stability in long-term electrolysis processes. Due to significant technological advancements in the recent years, interfacial investigation under reaction control is now increasingly feasible.^{30,87–90} There are several implications from many fundamental studies that may play key roles in determining the reaction mechanism as described above; participation of tin oxide for high FE (activity and selectivity), control of solution pH and applied potentials for high stability of catalysts, and size effect of nano-structured SnO₂ catalysts on activity. However, a direct observation that monitors simultaneous dynamic changes in structures and chemical properties of nano-catalyst surfaces under electrochemical reaction condition are still in the early stage. *Operando* Raman spectroscopy, in this context, is a promising technique that can provide real-time chemical information of nanostructured catalyst properties, allowing us to establish correlations between structure, activity, and stability of SnO₂ and its selectivity toward formate formation.⁸⁹

Operando Raman Study on Electrochemical Reduction of CO₂

In a previous work we conducted *operando* Raman spectroscopic studies using a home-made spectro-electrochemical cell, equipped with a quartz window on top, two inlets for solution exchange and gas purging, respectively, and one outlet of electrolyte/gas. A glassy carbon substrate (covered with drop-cast catalyst) was used as working, a Pt wire as counter, and an Ag/AgCl as reference electrode (Fig. 3). The spectro-electrochemical cell was connected to a glass wash bottle where the electrolyte solution (0.5 mol dm^{−3} NaOH) was deaerated with Ar gas and then its pH was tuned by bubbling CO₂ gas before the solution was introduced to the cell.

Raman measurements were carried out with a LabRAM HR-800 confocal Raman microscope (Horiba Jobin Ivon). A long working distance objective lens (50 times magnification, 8 mm focal length; Olympus) with a numerical aperture of 0.5 was used to focus DPSS laser (excitation wavelength 532 nm, power 1 mW) on the sample surface. The Raman signals were collected in a back-scattering geometry.

In order to observe the chemical changes of a real catalyst under reaction conditions, reduced graphene oxide (rGO)-supported SnO₂ nanoparticles (SnO₂ NPs) were synthesized. Using this catalyst, electrolysis of CO₂ was performed in aqueous solutions of different pH values. Previous studies in the literature revealed that the stability of tin oxides depends heavily both on the pH and the applied electrode potential.^{14,91} Therefore, measurements were carried out with slight or heavy alkaline solutions in the pH range between 8.5 and 12, which were prepared by controlling CO₂ bubbling time through a 0.5 mol dm^{−3} NaOH solution until the desired pH was achieved.

Electrochemical study of SnO₂ NPs catalyst was performed using linear sweep voltammetry in alkaline aqueous solutions with four different pH values (8.5, 9.7, 12, and 13.5). In general, the cathodic voltammetric response indicates three parallel processes taking place on SnO₂ surfaces. These are (1) the reduction of CO₂ yielding formate as a main product, (2) the hydrogen evolution reaction, dominantly taking place at $E < -1.5$ V versus Ag/AgCl, and (3) the reduction of SnO₂ catalyst forming tin species with lower oxidation numbers (Sn(II) or Sn(0), which was verified by means of XRD measurements⁸⁹).

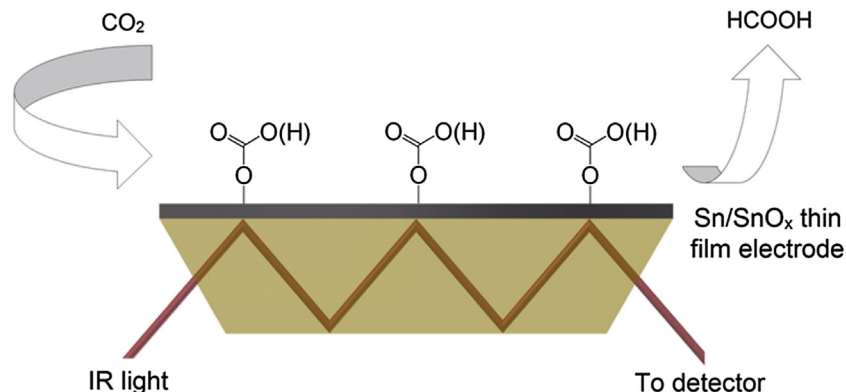


Fig. 2 Schematic diagram of ATR-IR spectroscopic study on formate formation from the electroreduction of CO₂ on Sn/SnO₂ thin film electrode. Reprint with permission from Won, D.H.; Choi, C.H.; Chung, J.; Chung, M.W.; Kim, E.H.; Woo, S.I. Rational Design of a Hierarchical Tin Dendrite Electrode for Efficient Electrochemical Reduction of CO₂. *ChemSusChem* **2015**, *8*, 3092–3098. Copyright 2015 American Chemical Society.

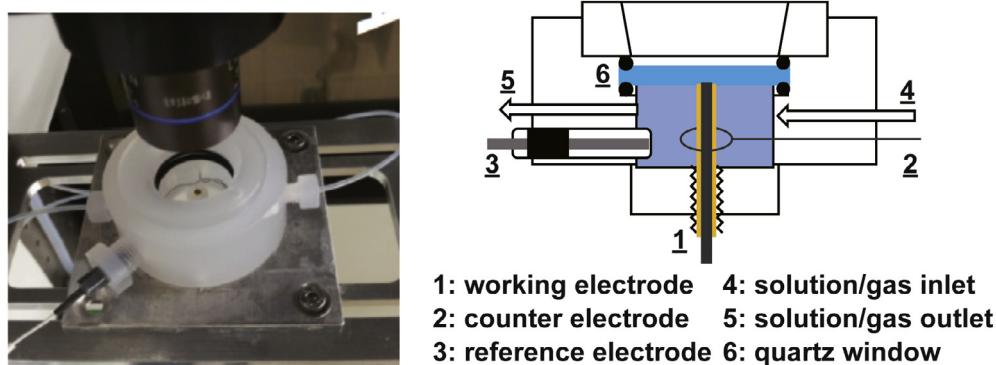


Fig. 3 Schematic diagram and photo image of homemade spectro-electrochemical cell used for *operando* Raman spectroscopic study.

The onset of reduction currents remains at approximately -0.9 V at all three pH levels, which can be attributed to the electroreduction of bicarbonate species in the aqueous solution as mentioned in literature (Fig. 4).^{82,91} The disappearance of this onset region is observed in base electrolytes not containing CO_2 (pH: 13.5).

In order to investigate the degradative reduction of SnO_2 to Sn and its effect on catalytic activity and selectivity, *operando* Raman spectroscopic studies were carried out under the same electrochemical conditions.

First we note that the normal Raman spectrum of SnO_2 NPs recorded in Ar atmosphere shows three distinctive Raman signals at 474 , 629 , and 768 cm^{-1} , which are assigned to the E_g , A_{1g} , and B_{2g} modes of SnO_2 (Fig. 4).^{92–96} SnO_2 has a tetragonal rutile crystalline structure, which belongs to the space group D_{4h}^{14} , and its unit cell consists of 4 oxygen atoms and 2 tin atoms. These 6 atoms in the unit cell yield in total 18 branches for the vibrational modes in the first Brillouin zone, and among them, the active Raman modes are a doubly degenerated E_g and three nondegenerated modes A_{1g} , B_{1g} , and B_{2g} . The latter three modes vibrate in the plane perpendicular to the c axis while the former mode vibrates in the direction of the c axis. The B_{1g} mode consists of rotation of oxygen atoms around the c axis, with all oxygen atoms of the octahedra participating in the vibration.⁹²

A detailed Raman study of SnO_2 nanoparticles was reported as a function of nanoparticle size.⁹⁴ It is claimed that when the size of the SnO_2 crystal is reduced, the infrared and Raman spectra are modified due to the size of the SnO_2 grain. Literature also points out the presence of new bands in SnO_2 NPs, which were not observed for single-crystal SnO_2 , although there is no clear explanation as to the origin of these bands. In addition to the main Raman peaks, three weak Raman peaks at 303 , 559 , and 692 cm^{-1} are observed in the normal Raman spectrum of SnO_2 NPs. The situation is similar to that reported by Sun et al. who studied single-crystalline rutile SnO_2 nanobelts observing two additional peaks at 313 and 690 cm^{-1} .⁹⁷ Abello et al. proposed that the Raman spectral signature changes drastically with the size of the particles. In particular, as the size of the SnO_2 decreases, the symmetry-forbidden infrared modes can become weakly active, together with the shift and broadening of the fundamental three peaks in the Raman spectra.⁹⁸ Ocaña et al. related the Raman peak at 310 cm^{-1} to a surface defect or some new kind of vibration mode arising as a result of SnO_2 nanocluster formation.^{99,100} On the other hand, the Raman signal at 559 cm^{-1} was proposed to appear as a consequence of reducing particle dimensions, which was assigned to a surface layer of nonstoichiometric SnO_2 with different symmetries than SnO_2 .^{92,96}

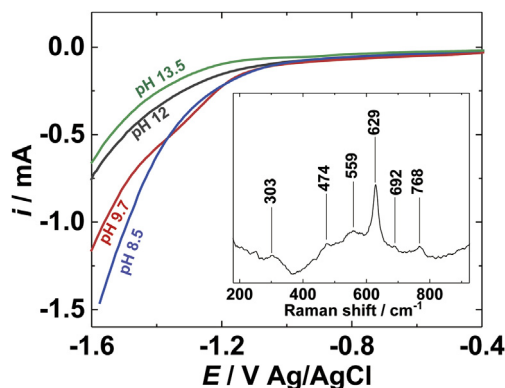


Fig. 4 Linear sweep voltammograms showing the pH dependence on the cathodic current while CO_2 is reduced on SnO_2 NPs. Inset: Normal Raman spectrum of SnO_2 NPs, as-prepared. Replot and reprint with permission from Dutta, A.; Kuzume, A.; Rahaman, M.; Veszteg, S.; Broekmann, P. Monitoring the Chemical State of Catalysts for CO_2 Electroreduction: An in *Operando* Study. *ACS Catal.* **2015**, *5*, 7498–7502. Copyright 2015, American Chemical Society.

The potential dependent steady-state Raman spectra recorded under *operando* conditions show three distinctive Raman signals due to E_g , A_{1g} , and B_{2g} modes in all electrolyte solutions (Fig. 5, upper panel). In the same potential range for catalytic reaction of CO_2 reduction, SnO_2 could also be reduced to metallic Sn.⁸² It is difficult to separate the true catalytic current for CO_2 reduction on SnO_2 from the overlapped parallel degradative reduction current of SnO_2 itself to metallic Sn.

To visualize these changes, the integrated intensity of the main peak at 628 cm^{-1} was plotted against the applied electrode potentials for pH 8.5, pH 9.7, and pH 12.0 respectively (Fig. 5, middle panel). Three potential regions labeled I to III can be distinguished as (I) the region of native SnO_2 phase; (II) the intermediate region where SnO_2 NPs are partially (20%–25%) reduced to metallic Sn; and (III) the region after complete reduction of SnO_2 to metallic Sn. The conversion from region I to II takes place around -0.5 V versus Ag/AgCl in the pH 8.5 solution, while it appears at -0.7 and -0.8 V in solutions of pH = 9.7 and 12.0, respectively. The normalized intensity values in region II are around 75%–80% of that in region I and shows a plateau down to $E < -1.4\text{ V}$.

By combining product analysis using gas and ion-exchange chromatographies, formate and CO concentration, together with the FE values for formate production, were obtained as a function of potential and pH of the solution (Fig. 5, lower panel).

By comparing the measured FEs (production selectivity of SnO_2) with the results of Raman spectroscopy (degradation of SnO_2), we found that the FE of formate production strongly depends on the oxidation state of the catalyst surface. At moderately cathodic potentials, the FE is increasing with decreasing electrode potentials (E); however as E tends to be more negative, this tendency breaks and the FE curves go over a maximum. At very negative potentials, where catalysts are completely reduced to metallic Sn, the FE for the formate production and the intensity of A_{1g} peaks are both heavily decreased. Interestingly, the maxima of the FE curves are at such potentials where the thermodynamically stable phase should be metallic Sn⁹¹; however, the reduction of the SnO_2 NPs is

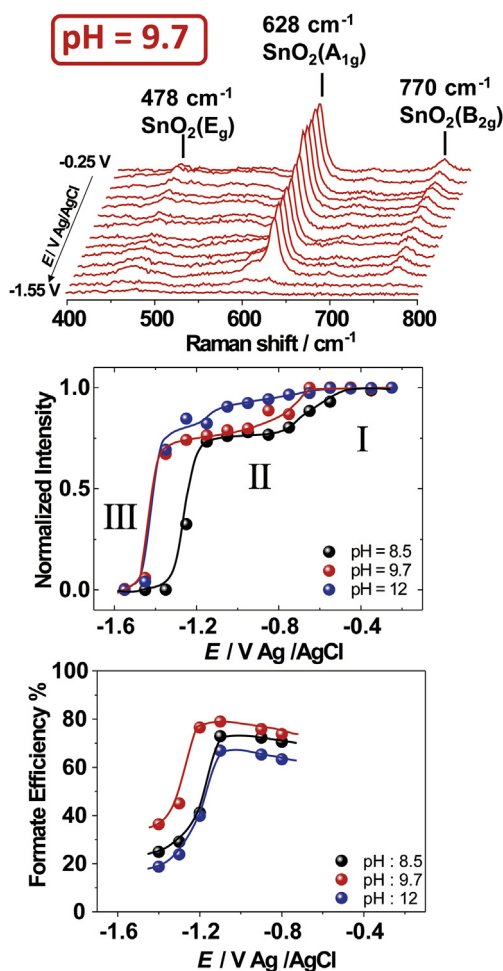


Fig. 5 Potential dependent *operando* Raman study at varied potential and pH. (Upper) The potential dependence of Raman spectra at pH 9.7 (middle) the relative intensity of A_{1g} Raman peak and (bottom) the FE values as a function of applied potentials. In the three distinct potential regions, catalyst is in the form of fully oxidized SnO_2 (I), a partially reduced compound of mixed oxidation state (II) and completely reduced metallic Sn^0 (III) illustrated in the middle panel. Redrawn plots from the data in Dutta, A.; Kuzume, A.; Rahaman, M.; Veszteg, S.; Broekmann, P. Monitoring the Chemical State of Catalysts for CO_2 Electrorreduction: An *Operando* Study. *ACS Catal.* **2015**, *5*, 7498–7502. Copyright 2015, American Chemical Society.

kinetically hindered. As a consequence, the Raman peak of SnO_2 is still of considerable intensity, indicating that the catalyst is only partially reduced and the SnO_2 phase is still prevalent. Similar conclusion was found in some literature reports stating that the presence of a surface oxide or a metal/metal oxide composite may play a significant role in the catalytic activity of CO_2 reduction on Sn electrodes.^{14,52}

Conclusion

By an *operando* Raman spectroscopic survey of SnO_2 NPs, a strong correlation has been established between the chemical state of catalysts (oxidation state of SnO_2) and their catalytic selectivity (FE for the formate production). The highest selectivity for the production of formate in alkaline CO_2 solution was found in a potential range where the SnO_2 phase is metastable and the SnO_2 -related Raman signals are mildly decreased, indicating that an only partial reduction of the SnO_2 surface is crucial for the production of formate with high activity and selectivity.

It is notable that the practical kinetic stability region of SnO_2 well exceeds the thermodynamic stability window (determined based on the Pourbaix diagram⁹¹) under these operating conditions. High FE for formate production was followed by a heavy drop in FE values when the applied potential is negative enough to fully reduce SnO_2 to metallic Sn, supporting that the Sn/ SnO_2 composite plays a significant role in CO_2 electroreduction.

In a more general context, we clearly demonstrated the applicability of *operando* Raman spectroscopy for understanding chemical and morphology changes that catalysts themselves can undergo during the catalyzed process.

See also: Electrochemical Surface Science of CO_2 Reduction at Well-Defined Cu Electrodes: Surface Characterization by Emersion, Ex Situ, In Situ, and Operando Methods; Enzymatic Electrocatalysis of CO_2 Reduction; Metal Oxide Cluster and Polyoxometallate Supports for Noble Metal Nanoparticles in Efficient Electrocatalysis.

References

- Arrhenius, S. On the Influence of Carbonic Acid in the Air upon the Temperature of the Ground. *Phil. Mag.* **1896**, *41*, 237–276.
- Karl, T. R.; Trenberth, K. E. Modern Global Climate Change. *Science* **2003**, *302*, 1719–1723.
- Oloman, C.; Li, H. Electrochemical Processing of Carbon Dioxide. *ChemSusChem* **2008**, *1*, 385–391.
- Kondratenko, E. V.; Mul, G.; Baltrusaitis, J.; Larrazabal, G. O.; Perez-Ramirez, J. Status and Perspectives of CO_2 Conversion Into Fuels and Chemicals by Catalytic, Photocatalytic and Electrocatalytic Processes. *Energy Environ. Sci.* **2013**, *6*, 3112–3135.
- Kang, P.; Cheng, C.; Chen, Z.; Schauer, C. K.; Meyer, T. J.; Brookhart, M. Selective Electrocatalytic Reduction of CO_2 to Formate by Water-Stable Iridium Dihydride Pincer Complexes. *J. Am. Chem. Soc.* **2012**, *134*, 5500–5503.
- Lewis, N. S.; Nocera, D. G. Powering the Planet: Chemical Challenges in Solar Energy Utilization. *Proc. Natl. Acad. Sci.* **2006**, *103*, 15729–15735.
- Angamuthu, R.; Byers, P.; Lutz, M.; Spek, A. L.; Bouwman, E. Electrocatalytic CO_2 Conversion to Oxalate by a Copper Complex. *Science* **2010**, *327*, 313–315.
- Boot-Handford, M. E.; Abanades, J. C.; Anthony, E. J.; Blunt, M. J.; Brandani, S.; MacDowell, N.; Fernandez, J. R.; Ferrari, M. C.; Gross, R.; Hallett, J. P.; Haszeldine, R. S.; Heptonstall, P.; Lyngfelt, A.; Makuch, Z.; Mangano, E.; Porter, R. T. J.; Pourkashanian, M.; Rochelle, G. T.; Shah, N.; Yao, J. G.; Fennell, P. S. Carbon Capture and Storage Update. *Energy Environ. Sci.* **2014**, *7*, 130–189.
- Durst, J.; Rudnev, A.; Dutta, A.; Fu, Y.; Herranz, J.; Kaliginedi, V.; Kuzume, A.; Permyakova, A. A.; Paratcha, Y.; Broekmann, P.; Schmidt, T. Electrochemical CO_2 Reduction—A Critical View on Fundamentals, Materials and Applications. *Chimia* **2015**, *69*, 769–776.
- Vo, T.; Purohit, K.; Nguyen, C.; Biggs, B.; Mayoral, S.; Haan, J. L. Formate: An Energy Storage and Transport Bridge Between Carbon Dioxide and a Formate Fuel Cell in a Single Device. *ChemSusChem* **2015**, *8*, 3853–3858.
- Kopljär, D.; Inan, A.; Vindayer, P.; Scholz, R.; Frangos, N.; Wagner, N.; Klemm, E. Development and Utilization of Gas Diffusion Electrodes for the Electrochemical Reduction of CO_2 . *Chem. Ing. Tech.* **2015**, *87*, 855–859.
- Bumroongsakulsawat, P.; Kelsall, G. H. Tinned Graphite Felt Cathodes for Scale-Up of Electrochemical Reduction of Aqueous CO_2 . *Electrochim. Acta* **2015**, *159*, 242–251.
- Parajuli, R.; Gerken, J. B.; Keyshar, K.; Sullivan, I.; Sivasankar, N.; Teamey, K.; Stahl, S. S.; Cole, E. B. Integration of Anodic and Cathodic Catalysts of Earth-Abundant Materials for Efficient, Scalable CO_2 Reduction. *Top. Catal.* **2015**, *58*, 57–66.
- Lee, S.; Ju, H. K.; Machunda, R.; Uhm, S.; Lee, J. K.; Lee, H. J.; Lee, J. Sustainable Production of Formic Acid by Electrolytic Reduction of Gaseous Carbon Dioxide. *J. Mater. Chem. A* **2015**, *3*, 3029–3034.
- Wang, Q. N.; Dong, H.; Yu, H. B.; Yu, H.; Liu, M. H. Enhanced Electrochemical Reduction of Carbon Dioxide to Formic Acid Using a Two-Layer Gas Diffusion Electrode in a Microbial Electrolysis Cell. *RSC Adv.* **2015**, *5*, 10346–10351.
- Wang, Q. N.; Dong, H.; Yu, H. B. Development of Rolling Tin Gas Diffusion Electrode for Carbon Dioxide Electrochemical Reduction to Produce Formate in Aqueous Electrolyte. *J. Power Sources* **2014**, *271*, 278–284.
- Amao, Y.; Shuto, N. Formate Dehydrogenase—Viologen-Immobilized Electrode for CO_2 Conversion, for Development of an Artificial Photosynthesis System. *Res. Chem. Intermed.* **2014**, *40*, 3267–3276.
- Wang, Q. N.; Dong, H.; Yu, H. B. Fabrication of a Novel Tin Gas Diffusion Electrode for Electrochemical Reduction of Carbon Dioxide to Formic Acid. *RSC Adv.* **2014**, *4*, 59970–59976.
- Agarwal, A. S.; Zhai, Y. M.; Hill, D.; Sridhar, N. The Electrochemical Reduction of Carbon Dioxide to Formate/Formic Acid: Engineering and Economic Feasibility. *ChemSusChem* **2011**, *4*, 1301–1310.
- Wang, Y. J.; Chandler, W. The Chinese Nonferrous Metals Industry-Energy Use and CO_2 Emissions. *Energy Policy* **2010**, *38*, 6475–6484.
- Li, H. and Oloman, C. (206) “Development of a Continuous Reactor for the Electroreduction of Carbon Dioxide to Formate—Part 1: Process Variables”, *J. Appl. Electrochem.* **36**, 1105–1115.
- Subramanian, K.; Asokan, K.; Jeevarathinam, D.; Chandrasekaran, M. Electrochemical Membrane Reactor for the Reduction of Carbon Dioxide to Formate. *J. Appl. Electrochem.* **2007**, *37*, 255–260.
- Royer, M. E. Reduction de l'acide carbonique en acide formique. *C. R. Hebd. Seances Acad. Sci.* **1870**, *70*, 731–732.

24. Hori, Y.; Wakebe, H.; Tsukamoto, T.; Koga, O. Electrocatalytic Process of CO Selectivity in Electrochemical Reduction of CO₂ at Metal Electrodes in Aqueous Media. *Electrochim. Acta* **1997**, *39*, 1833–1839.
25. Jones, J.-P.; Surya Prakash, G. K.; Olah, G. A. Electrochemical CO₂ Reduction: Recent Advances and Current Trends. *Isr. J. Chem.* **2014**, *54*, 1451–1466.
26. MaQuillan, A. J.; Hendra, P. J.; Fleischman, M. Raman Spectroscopic Investigation of Silver Electrodes. *J. Electroanal. Chem.* **1975**, *65*, 933–944.
27. Gibson, D. H. Carbon Dioxide Coordination Chemistry: Metal Complexes and Surface-Bound Species. What Relationships? *Coord. Chem. Rev.* **1999**, *185–186*, 335–355.
28. Amatore, C.; Saveant, J. M. Mechanism and Kinetic Characteristics of the Electrochemical Reduction of Carbon Dioxide in Media of Low Proton Availability. *J. Am. Chem. Soc.* **1981**, *103*, 5021–5023.
29. Pacansky, J.; Wahlgren, U.; Bagus, P. S. SCF Ab-Initio Ground State Energy Surfaces for CO₂ and CO₂[−]. *J. Chem. Phys.* **1975**, *62*, 2740–2744.
30. Mistry, H.; Varela, A. S.; Bonifacio, C. S.; Zegkinoglou, I.; Sinev, I.; Choi, Y. W.; Kisslinger, K.; Stach, E. A.; Yang, J. C.; Strasser, P.; Cuenya, B. R. Highly Selective Plasma-Activated Copper Catalysts for Carbon Dioxide Reduction to Ethylene. *Nat. Commun.* **2016**, *7*, 12123.
31. Rosen, B. A.; Salehi-Khojin, A.; Thorson, M. R.; Zhu, W.; Whipple, D. T.; Kenis, P. J.; Masel, R. I. Ionic Liquid-Mediated Selective Conversion of CO₂ to CO at Low Overpotentials. *Science* **2011**, *334*, 643–644.
32. Hori, Y. Electrochemical CO₂ Reduction on Metal Electrodes. In *Modern Aspects of Electrochemistry* 42; Vayenas, C. G., White, R. E., Gamboa-Aldeco, M. E., Eds.; Springer: Greece, 2008; pp 89–189.
33. Hoshi, N.; Kato, M.; Hori, Y. Electrochemical Reduction of CO₂ on Single Crystal Electrodes of Silver Ag(111), Ag(100) and Ag(110). *J. Electroanal. Chem.* **1997**, *440*, 283–286.
34. Sarfraz, S.; Garcia-Esparza, A. T.; Jedidi, A.; Cavallo, L.; Takanabe, K. Cu–Sn Bimetallic Catalyst for Selective Aqueous Electroreduction of CO₂ to CO. *ACS Catal.* **2016**, *6*, 2842–2851.
35. Su, Z. J.; Zhang, Y. B.; Liu, B. B.; Zhou, Y. L.; Jiang, T.; Li, G. H. Reduction Behaviour of SnO₂ in the Tin-Bearing Iron Concentrates under CO–CO₂ Atmosphere. Part 1: Effect of Magnetite. *Powder Technol.* **2016**, *292*, 251–259.
36. Choi, S. Y.; Jeong, S. K.; Kim, H. J.; Baek, I. H.; Park, K. T. Electrochemical Reduction of Carbon Dioxide to Formate on Tin-Lead Alloys. *ACS Sustain. Chem. Eng.* **2016**, *4*, 1311–1318.
37. Yadav, V. S. K.; Purkait, M. K. Solar Cell Driven Electrochemical Process for the Reduction of CO₂ to HCOOH on Zn and Sn Electrocatalysts. *Solar Energy* **2016**, *124*, 177–183.
38. Wang, Y.; Zhou, J.; Lv, W. X.; Fang, H. L.; Wang, W. Electrochemical Reduction of CO₂ to Formate Catalysed by Electroplated Tin Coating on Copper Foam. *Appl. Surf. Sci.* **2016**, *362*, 394–398.
39. Lv, W. X.; Zhou, J.; Kong, F. Y.; Fang, H. L.; Wang, W. Porous Tin-Based Film Deposited on Copper Foil for Electrochemical Reduction of Carbon Dioxide to Formate. *Int. J. Hydrogen Energy* **2016**, *41*, 1585–1591.
40. Zhao, Y.; Wang, C. Y.; Wallace, G. G. Tin Nanoparticles Decorated Copper Oxide Nanowires for Selective Electrochemical Reduction of Aqueous CO₂ to CO. *J. Mater. Chem. A* **2016**, *4*, 10710–10718.
41. Zhu, W.; Ke, J.; Wang, S. B.; Ren, J.; Wang, H. H.; Zhou, Z. Y.; Si, R.; Zhang, Y. W.; Yan, C. H. Shaping Single-Crystalline Trimetallic Pt–Pd–Rh Nanocrystals Toward High-Efficiency C–C Splitting of Ethanol in Conversion of CO₂. *ACS Catal.* **2015**, *5*, 1995–2008.
42. Gerales, A. N.; da Silva, D. F.; da Silva, J. C. M.; de Sa, O. A.; Spinace, E. V.; Neto, A. O.; dos Santos, M. C. Palladium and Palladium-Tin Supported on Multi Wall Carbon Nanotubes or Carbon for Alkaline Direct Ethanol Fuel Cell. *J. Power Sources* **2015**, *275*, 189–199.
43. Yadav, V. S. K.; Purkait, M. K. Electrochemical Reduction of CO₂ to HCOOH Using Zinc and Cobalt Oxide as Electrocatalysts. *New J. Chem.* **2015**, *39*, 7348–7354.
44. Cherashev, A. F.; Khrushch, A. P. Electrochemical Reduction of Carbon Dioxide on Tin, Zinc, and Their Alloys. *Russ. J. Electrochem.* **1998**, *34*, 410–417.
45. Cherashev, A. F.; Khrushch, A. P. The Electrochemical Reduction of Carbon Dioxide at the Tin-Cadmium and Tin-Zinc Alloys. *Russ. J. Electrochem.* **1997**, *33*, 181–185.
46. Bei, J. J.; Zhang, R.; Chen, Z. D.; Lv, W. X.; Wang, W. Efficient Reduction of CO₂ to Formate Using In Situ Prepared Nano-Sized Bi Electrocatalyst. *Int. J. Electrochem. Sci.* **2017**, *12*, 2365–2375.
47. Cui, C. N.; Han, J. Y.; Zhu, X. L.; Liu, X.; Wang, H.; Mei, D. H.; Ge, Q. F. Promotional Effect of Surface Hydroxyls on Electrochemical Reduction of CO₂ over SnO₂/Sn Electrode. *J. Catal.* **2016**, *343*, 257–265.
48. Larrazabal, G. O.; Martin, A. J.; Mitchell, S.; Hauert, R.; Perez-Ramirez, J. Synergistic Effects in Silver-Indium Electrocatalysts for Carbon Dioxide Reduction. *J. Catal.* **2016**, *343*, 266–277.
49. Azuma, M.; Hashimoto, K.; Hiramoto, M.; Watanabe, M.; Sakata, T. Electrochemical Reduction of Carbon Dioxide on Various Metal Electrodes in Low-Temperature Aqueous KHCO₃ Media. *J. Electrochem. Soc.* **1990**, *137*, 1772–1778.
50. Qiao, J.; Liu, Y.; Hong, F.; Zhang, J. A Review of Catalysts for the Electroreduction of Carbon Dioxide to Produce Low-Carbon Fuels. *Chem. Soc. Rev.* **2014**, *43*, 631–675.
51. Li, C. W.; Ciston, J.; Kanan, M. W. Electroreduction of Carbon Monoxide to Liquid Fuel on Oxide-Derived Nanocrystalline Copper. *Nature* **2014**, *508*, 504–507.
52. Chen, Y.; Kanan, M. W. Tin Oxide Dependence of the CO₂ Reduction Efficiency on Tin Electrodes and Enhanced Activity for Tin/Tin Oxide Thin-Film Catalysts. *J. Am. Chem. Soc.* **2012**, *134*, 1986–1989.
53. Li, C. W.; Kanan, M. W. CO₂ Reduction at Low Overpotential on Cu Electrodes Resulting From the Reduction of Thick Cu₂O Films. *J. Am. Chem. Soc.* **2012**, *134*, 7231–7234.
54. White, J. L.; Bocarsly, A. B. Enhanced Carbon Dioxide Reduction Activity on Indium-Based Nanoparticles. *J. Electrochem. Soc.* **2016**, *163*, H410–H416.
55. Chen, L.; Guo, S. X.; Li, F. W.; Bentley, C.; Horne, M.; Bond, A. M.; Zhang, J. Electrochemical Reduction of CO₂ at Metal Electrodes in a Distillable Ionic Liquid. *ChemSusChem* **2016**, *9*, 1271–1278.
56. Detweiler, Z. M.; White, J. L.; Bernasek, S. L.; Bocarsly, A. B. Anodized Indium Metal Electrodes for Enhanced Carbon Dioxide Reduction in Aqueous Electrolyte. *Langmuir* **2014**, *30*, 7593–7600.
57. Zhang, R.; Lv, W. X.; Lei, L. X. Role of Oxide Layer on Sn Electrode in Electrochemical Reduction of CO₂ to Formate. *Appl. Surf. Sci.* **2015**, *356*, 24–29.
58. Lv, W. X.; Zhang, R.; Gao, P.; Lei, L. Studies on the Faradaic Efficiency for Electrochemical Reduction of Carbon Dioxide to Formate on Tin Electrode. *J. Power Sources* **2014**, *253*, 276–281.
59. Alvarez-Guerra, M.; Del Castillo, A.; Irabien, A. Continuous Electrochemical Reduction of Carbon Dioxide Into Formate Using a Tin Cathode: Comparison With Lead Cathode. *Chem. Eng. Res. Des.* **2014**, *92*, 692–701.
60. Koleli, F.; Atilan, T.; Palamut, N.; Gizir, A. M.; Aydin, R.; Hamann, C. H. Electrochemical Reduction of CO₂ at Pb- and Sn-Electrodes in a Fixed-Bed Reactor in Aqueous K₂CO₃ and KHCO₃ Media. *J. Appl. Electrochem.* **2003**, *33*, 447–450.
61. Chiacchiarelli, L. M.; Zhai, Y.; Frankel, G. S.; Agarwal, A. S.; Sridhar, N. Cathodic Degradation Mechanisms of Pure Sn Electrocatalyst in a Nitrogen Atmosphere. *J. Appl. Electrochem.* **2012**, *42*, 21–29.
62. Li, Y. A.; Qiao, J. L.; Zhang, X.; Lei, T.; Girma, A.; Liu, Y. Y.; Zhang, J. J. Rational Design and Synthesis of SnO_x Electrocatalysts With Coralline Structure for Highly Improved Aqueous CO₂ Reduction to Formate. *Chem. Commun.* **2016**, *3*, 1618–1628.
63. Wu, J. J.; Risalvato, F. G.; Ma, S.; Zhou, X. D. Electrochemical Reduction of Carbon Dioxide III. The Role of Oxide Layer Thickness on the Performance of Sn Electrode in a Full Electrochemical Cell. *J. Mater. Chem. A* **2014**, *2*, 1647–1651.
64. Wu, J. J.; Risalvato, F. G.; Ke, F. S.; Pellechia, P. J.; Zhou, X. D. Electrochemical Reduction of Carbon Dioxide I. Effects of the Electrolyte on the Selectivity and Activity With Sn Electrode. *J. Electrochem. Soc.* **2012**, *159*, F353–F359.
65. Fu, Y. S.; Li, Y. N.; Zhang, X.; Liu, Y. Y.; Qiao, J. L.; Zhang, J. J.; Wilkinson, D. P. Novel Hierarchical SnO₂ Microsphere Catalyst Coated on Gas Diffusion Electrode for Enhancing Energy Efficiency of CO₂ Reduction to Formate Fuel. *Appl. Energy* **2016**, *175*, 536–544.

66. Fu, Y. S.; Li, Y. N.; Zhang, X.; Liu, Y. Y.; Zhou, X. D.; Qiao, J. L. Electrochemical CO₂ Reduction to Formic Acid on Crystalline SnO₂ Nanosphere Catalyst With High Selectivity and Stability. *Chin. J. Catal.* **2016**, *37*, 1081–1088.
67. Zhao, C. C.; Wang, J. L. Electrochemical Reduction of CO₂ to Formate in Aqueous Solution Using Electro-Deposited Sn Catalysts. *Chem. Eng. J.* **2016**, *293*, 161–170.
68. Machunda, R. L.; Ju, H.; Lee, J. Electrocatalytic Reduction of CO₂ Gas at Sn Based Gas Diffusion Electrode. *Curr. Appl. Phys.* **2011**, *11*, 986–988.
69. Kumar, B.; Atia, V.; Brian, J. P.; Kumari, S.; Nguyen, T. Q.; Sunkara, M.; Spurgeon, J. M. Reduced SnO₂ Porous Nanowires With a High Density of Grain Boundaries as Catalysts for Efficient Electrochemical CO₂-into-HCOOH Conversion. *Angew. Chem., Int. Ed.* **2017**, *56*, 3645–3649.
70. Del Castillo, A.; Alvarez-Guerra, M.; Solla-Gullon, J.; Saez, A.; Montiel, V.; Irabien, A. Electrocatalytic Reduction of CO₂ to Formate Using Particulate Sn Electrodes: Effect of Metal Loading and Particle Size. *Appl. Energy* **2015**, *157*, 165–173.
71. Wu, J. J.; Sharma, P. P.; Harris, B. H.; Zhou, X. D. Electrochemical Reduction of Carbon Dioxide: IV Dependence of the Faradaic Efficiency and Current Density on the Microstructure and Thickness of Tin Electrode. *J. Power Sources* **2014**, *258*, 189–194.
72. Zhao, C. C.; Wang, J. L.; Goodenough, J. B. Comparison of Electrocatalytic Reduction of CO₂ to HCOOH with Different Tin Oxides on Carbon Nanotubes. *Electrochem. Commun.* **2016**, *65*, 9–13.
73. Alagdal, I. A.; West, A. R. Oxygen Non-Stoichiometry, Conductivity and Gas Sensor Response of SnO₂ Pellets. *J. Mater. Chem. A* **2015**, *3*, 23213–23219.
74. Abanades, S. CO₂ and H₂O Reduction by Solar Thermochemical Looping Using SnO₂/SnO Redox Reactions: Thermogravimetric Analysis. *Int. J. Hydrogen Energy* **2012**, *37*, 8223–8231.
75. Zhang, Y. B.; Liu, B. B.; Su, Z. J.; Chen, J.; Li, G. H.; Jiang, T. Volatilization Behaviour of SnO₂ Reduced Under Different CO–CO₂ Atmospheres at 975°C–1100°C. *Int. J. Miner. Process.* **2015**, *144*, 33–39.
76. Mizuno, T.; Ohta, K.; Sasaki, A.; Akai, T.; Hirano, M.; Kawabe, A. Effect of Temperature on Electrochemical Reduction of High-Pressure CO₂ with in, Sn, and Pb Electrodes. *Energy Sources* **1995**, *17*, 503–508.
77. Scialdone, O.; Galia, A.; Lo Nero, G.; Proietto, F.; Sabatino, S.; Schiavo, B. Electrochemical Reduction of Carbon Dioxide to Formic Acid at a Tin Cathode in Divided and Undivided Cells: Effect of Carbon Dioxide Pressure and Other Operating Parameters. *Electrochim. Acta* **2016**, *199*, 332–341.
78. Anawati, Frankel, G. S.; Agarwal, A.; Sridhar, N. Degradation and Deactivation of Sn Catalyst Used for CO₂ Reduction as Function of Overpotential. *Electrochim. Acta* **2014**, *133*, 188–196.
79. Kopljär, D.; Inan, A.; Vindayer, P.; Wagner, N.; Klemm, E. Electrochemical Reduction of CO₂ to Formate at High Current Density Using Gas Diffusion Electrodes. *J. Appl. Electrochem.* **2014**, *44*, 1107–1116.
80. Bumroongsakulsawat, P.; Kelsall, G. H. Effect of Solution pH on CO: Formate Formation Rates During Electrochemical Reduction of Aqueous CO₂ at Sn Cathodes. *Electrochim. Acta* **2014**, *141*, 216–225.
81. Kim, H. Y.; Choi, I.; Ahn, S. H.; Hwang, S. J.; Yoo, S. J.; Han, J.; Kim, J.; Park, H.; Jang, J. H.; Kim, S. K. Analysis on the Effect of Operating Conditions on Electrochemical Conversion of Carbon Dioxide to Formic Acid. *Int. J. Hydrogen Energy* **2014**, *39*, 16506–16512.
82. Lee, S.; Ocon, J. D.; Son, Y.; Lee, J. Alkaline CO₂ Electrolysis Toward Selective and Continuous HCOO[−]—Production Over SnO₂ Nanocatalysts. *J. Phys. Chem. C* **2015**, *119*, 4884–4890.
83. Zhang, S. Nanostructured Tin Catalysts for Selective Electrochemical Reduction of Carbon Dioxide to Formate. *J. Am. Chem. Soc.* **2014**, *136*, 1734–1737.
84. Fu, Y.; Liu, Y.; Qiao, J.; Zhou, Z. D. Electrochemical CO₂ Reduction to Formic Acid on Crystalline SnO₂ Nanosphere Catalyst. *ECS Trans.* **2015**, *66*, 53–59.
85. Zhang, R.; Lv, W.; Li, G. H.; Lei, L. Electrochemical Reduction of CO₂ on SnO₂/Nitrogen-Doped Multiwalled Carbon Nanotubes Composites in KHCO₃ Aqueous Solution. *Mater. Lett.* **2015**, *141*, 63–65.
86. Won, D. H.; Choi, C. H.; Chung, J.; Chung, M. W.; Kim, E. H.; Woo, S. I. Rational Design of a Hierarchical Tin Dendrite Electrode for Efficient Electrochemical Reduction of CO₂. *ChemSusChem* **2015**, *8*, 3092–3098.
87. Baruch, M. F.; Panderill, J. E.; White, J. L.; Bocarsly, A. B. Mechanistic Insights Into the Reduction of CO₂ on Tin Electrodes Using In Situ ATR-IR Spectroscopy. *ACS Catal.* **2015**, *5*, 3148–3156.
88. Pander, J. E.; Baruch, M. F.; Bocarsly, A. B. Probing the Mechanism of Aqueous CO₂ Reduction on Post-Transition-Metal Electrodes Using ATR-IR Spectroelectrochemistry. *ACS Catal.* **2016**, *6*, 7824–7833.
89. Dutta, A.; Kuzume, A.; Rahaman, M.; Veszteg, S.; Broekmann, P. Monitoring the Chemical State of Catalysts for CO₂ Electroreduction: An in Operando Study. *ACS Catal.* **2015**, *5*, 7498–7502.
90. Choi, Y. W.; Mistry, H.; Cuenya, B. R. New Insights Into Working Nanostructured Electrocatalysts Through Operando Spectroscopy and Microscopy. *Curr. Opin. Electrochem* **2017**, *1*, 95–103.
91. Pourbaix, M. *Atlas d'équilibres électrochimique*, Gauthier-Villars et Cie: Paris, 1963; p 479.
92. Dieguez, A.; Romano-Rodriguez, A.; Vila, A.; Morante, J. R. The Complete Raman Spectrum of Nanometric SnO₂ Particles. *J. Appl. Phys.* **2001**, *90*, 1550–1557.
93. Jian, J. K.; Chen, X. L.; Xu, T.; Xu, Y. P.; Dai, L.; He, M. Synthesis, Morphologies and Raman-Scattering Spectra of Crystalline Stannic Oxide Nanowires. *Appl. Phys. A: Mater. Sci. Process.* **2002**, *75*, 695–697.
94. Rumyantseva, M. N.; Gaskov, A. M.; Rosman, N.; Pagnier, T.; Morante, J. R. Raman Surface Vibration Modes in Nanocrystalline SnO₂: Correlation With Gas Sensor Performances. *Chem. Mater.* **2005**, *17*, 893–901.
95. Palacios-Padros, A.; Caballero-Briones, F.; Diez-Perez, I.; Sanz, F. Tin Passivation in Alkaline Media: Formation of SnO Microcrystals as Hydroxyl Etching Product. *Electrochim. Acta* **2013**, *111*, 837–845.
96. Vijayarangamuthu, K.; Rath, S. Nanoparticle Size, Oxidation State, and Sensing Response of Tin Oxide Nanopowders Using Raman Spectroscopy. *J. Alloys Compd.* **2014**, *610*, 706–712.
97. Sun, S. H.; Meng, G. W.; Zhang, G. X.; Gao, T.; Geng, B. Y.; Zhang, L. D.; Zuo, J. Raman Scattering Study of Rutile SnO₂ Nanobelts Synthesized by Thermal Evaporation of Sn Powders. *Chem. Phys. Lett.* **2003**, *376*, 103–107.
98. Abello, L.; Bochu, B.; Gaskov, A.; Koudryavtseva, S.; Lucazeau, G.; Roumyantseva, M. Structural Characterization of Nanocrystalline SnO₂ by X-Ray and Raman Spectroscopy. *J. Solid State Chem.* **1998**, *135*, 78–85.
99. Ocaña, M.; Serna, C. J.; Garcia-Ramos, J. V.; Matijevic, E. A Vibrational Study of Uniform SnO₂ Powders of Various Morphologies. *Solid State Ionics* **1997**, *63–65*, 170–177.
100. Yu, K. N.; Xiong, Y.; Liu, Y.; Xiong, C. Microstructural Change of Nano-SnO₂ Grain Assemblages With the Annealing Temperature. *Phys. Rev. B* **1997**, *55*, 2666–2671.

Further Reading

CO₂ Electroreduction on Sn/SnO₂

- Hori, Y.; Wakebe, H.; Tsukamoto, T.; Koga, O. Electrocatalytic Process of CO Selectivity in Electrochemical Reduction of CO₂ at Metal Electrodes in Aqueous Media. *Electrochim. Acta* **1997**, *39*, 1833–1839.
- Bumroongsakulsawat, P.; Kelsall, G. H. Effect of Solution pH on CO: Formate Formation Rates During Electrochemical Reduction of Aqueous CO₂ at Sn Cathodes. *Electrochim. Acta* **2014**, *141*, 216–225.

- Lee, S.; Ocon, J. D.; Son, Y.; Lee, J. Alkaline CO₂ Electrolysis toward Selective and Continuous HCOO[−] Production over SnO₂ Nanocatalysts. *J. Phys. Chem. C* **2015**, *119*, 4884–4890.
- Baruch, M. F.; Pander, J. E.; White, J. L.; Bocarsly, A. B. Mechanistic Insights into the Reduction of CO₂ on Tin Electrodes Using In Situ ATR-IR Spectroscopy. *ACS Catal.* **2015**, *5*, 3148–3156.
- Choi, Y. W.; Mistry, H.; Cuenya, B. R. New Insights Into Working Nanostructured Electrocatalysts Through Operando Spectroscopy and Microscopy. *Curr. Opin. Electrochem.* **2017**, *7*, 95–103.

Raman Spectroscopy on Sn/SnO₂ Nanoparticle

- Rumyantseva, M. N.; Gaskov, A. M.; Rosman, N.; Pagnier, T.; Morante, J. R. Raman Surface Vibration Modes in Nanocrystalline SnO₂: Correlation With Gas Sensor Performances. *Chem. Mater.* **2005**, *17*, 893–901.
- Dieguez, A.; Romano-Rodríguez, A.; Vila, A.; Morante, J. R. The Complete Raman Spectrum of Nanometric SnO₂ Particles. *J. Appl. Phys.* **2001**, *90*, 1550–1557.
- Vijayarangamuthu, K.; Rath, S. Nanoparticle Size, Oxidation State, and Sensing Response of Tin Oxide Nanopowders Using Raman Spectroscopy. *J. Alloys Compd.* **2014**, *610*, 706–712.
- Medina-Ramos, J.; Pupillo, R. C.; Keane, T. P.; DiMeglio, J. L.; Rosenthal, J. Efficient Conversion of CO₂ to CO Using Tin and Other Inexpensive and Easily Prepared Post-Transition Metal Catalysts. *J. Am. Chem. Soc.* **2015**, *137*, 5021–5027.